Sustainable Water Resources Management (2020) 6:77
https://doi.org/10.1007/s40899-020-00436-1

ORIGINAL ARTICLE

Projections of future rainfall and temperature using statistical downscaling techniques in Tana Basin, Ethiopia

Hailu Birara[1] · R. P. Pandey[2] · S. K. Mishra[1]

Received: 23 August 2019 / Accepted: 10 August 2020 / Published online: 17 August 2020
© Springer Nature Switzerland AG 2020

Abstract
Global climate changes are becoming main threats to hydrological cycle, which thus influence environmental, social, and economic systems. Climate change studies using global climate models (GCMs) are mostly used for mitigation and adaptation strategies regarding the changing climate. The current GCMs' data are, however, too coarse to use directly at the regional and local scales for climate change studies. Two widely used statistical downscaling methods, namely LARS-WG and SDSM models, were used to study the current and future climate change of Tana Basin, Ethiopia. Four GCMs (GFCM21, HadCM3, MPEH5, and NCCCS) for LARS-WG and two GCMs (HadCM3 and CanESM2) for SDSM with different emission scenarios were evaluated. Overall results indicated an acceptable response of the models to simulate and forecast climatic variables under HadCM3 and CanESM2 GCMs. Rainfall results downscaled by LARS-WG from the four GCMs indicated high intermodal variabilities and non-consistence; Increasing trend of rainfall showed on three of the GCMs while one GCM showed a decreasing trend in the range of − 9.6% to 45.2%. The four GCMs rainfall average ensemble value showed an increasing trend ranging from 3.9% to 18.8%, which is also consistent with HadCM3 projections ranging from 4.1% to 19.2%. However, the downscaled results from all four models showed increasing maximum and minimum temperature for all time periods. The mean annual maximum and minimum temperature change increased from 0.9 °C to 2.9 °C and 0.6 °C to 2.5 °C, respectively, while annual mean relative change of rainfall ranged from 9.9% to 44.7%. Both SDSM and LARS-WG methods were obtained good monthly rainfall data series than daily rainfall data series in the study area. However, both models with the selected GCMs (HadCM3 and CanESM2) performed reasonably well to simulate temperature than rainfall.

Keywords Statistical downscaling model · GCMs · LARS-WG · SDSM · Tana basin · Ethiopia

Introduction

Climate change is becoming one of the significant environmental, economic, and social threats to the world. Since 1950, a decrease in the amount of snow, a heating ocean, and rising sea levels have been noticed as results of climate system warming (Intergovernmental Panel on Climate Change [IPCC] 2014). This changing climate affects water resources, especially in tropical regions (Beecham et al. 2014). The climate system has been influenced by human-induced forces activities for centuries. However, the impact of human activities started to extend to a global scale since the start of the industrial revolution (Cubasch et al. 2001; IPCC 2013). According to a 2013 IPCC report, global average temperature will rise between 1.4 °C and 5.8 °C by 2100 with a doubling of the CO2 concentration in the atmosphere. Sea-level rise, change in precipitation pattern (up to ± 20%), and change in other local climate conditions are also expected (Cubasch et al. 2001). Research has shown that warming is likely to occur faster in Africa, especially sub-Sahara countries, compared with the global average (Cubasch et al. 2001; Hulme et al. 2001). For example, even though the trend is different geographically, warming is occurring in almost all seasons as with the temperature and precipitation remains highly variable, unpredictable, and likely associated with changes in the climate (Conway et al. 2004). As a result, shifts in the crop-growing season and increased frequency of

✉ Hailu Birara
hailubirara@gmail.com

[1] Department of Water Resources Development and Management, Indian Institute of Technology Roorkee, Roorkee, Uttarakhand 247667, India

[2] National Institute of Hydrology Roorkee, Roorkee, Uttarakhand 247667, India

extreme events such as flood and drought are recent evidence of climate-change-related hazards in the region.

Because the entire African continent is the least studied region in terms of ecosystems dynamics, climate change, and its impact, the primary mechanisms associated with coupled climate-human-ecosystem changes are not well understood (Hely et al. 2006; IPCC 2013; Shongwe et al. 2009; Anyah and Qiu 2012; Endris et al. 2013). The IPCC (2013) report indicated that Ethiopia will be more vulnerable to climate change due to its less flexible economic structure and its dependence on rain-fed agriculture. Changes in seasonal patterns and precipitation distribution, timing, and pattern, as well as temperature, are already being witnessed in most parts of the country (Bewket and Conway 2007). In many parts of the country, precipitation is becoming more unpredictable every season and every year.

Tana Basin is one of the largest populated basins in the country and is highly dependent on a rain-fed agriculture economy, which may be influenced by the changing climate and variability of water resources (Setegn et al. 2011). Hence an assessment of the possible future impact of climate change in the region is needed to enhance the knowledge and understanding of the complex interaction between climate change and its potential effects on agro-ecological sectors that directly impact the livelihood of the large population of Ethiopia.

Climate models are appropriate tools for climate variability and change assessment (Endris et al. 2013). The global climate model (GCM) is a type of climate model used to simulate changes in atmospheric circulation and forecast climate changes (Shongwe et al. 2009). Nowadays, there is interest from a range of decision-makers and researchers in climate change information at a high spatial resolution on local and regional scales. However, their coarse resolution (100–250 km) prevents GCMs from capturing the detailed climatic processes at the regional and local scale (Giorgi et al. 2009). The coarser resolution also prevents GCMs from providing precise information about extreme events, which is of fundamental importance for users looking for climatic information to determine the regional-scale impact of climate variability and change.

Over the past years, many researchers used GCMs (IPCC 2013) to simulate past climate change and future climate projection (Christensen et al. 2007; Giorgi et al. 2009; Mearns 2009). World climate research programmers worked to organize the Coupled Model Intercomparison Project Phase (CMIP; Cubasch et al. 2001). Nowadays, a new generation of the CMIP (CMIP5) has proven to be a significant contribution to the IPCC AR5 report. In CMIP5, efforts included more complete representations of external forcing, more types of scenarios, more diagnostics, and higher resolution in a large number of models, compared with the climate models in CMIP3 that were used in the IPCC AR4 (Knutti and Sedláček 2013). CMIP5 comprises new scenarios, or representative concentration pathways (RCPs), which better reflect atmospheric concentrations of greenhouse gases in the climate change convention and promote understanding of the possible climate and future socioeconomic developments. Various studies of climate change projection have used the dataset of the climate model in CMIP5 with different RCPs and concluded that CMIP5 models performed better than CMIP3 models (Kharel and Kirilenko 2018; King et al. 2012; Kumar et al. 2014; Jha et al. 2014; Singh and Goyal 2016; Su et al. 2013; Wu et al. 2013). However, the GCMs are coarse scale and can hardly be applied directly to climate change and hydrological impact studies at the regional level (Tofiq and Guven 2014). To obtain the desired information in terms of hydrometeorological variables at a very fine spatial resolution or station scale, dynamic and statistical downscaling approaches have been developed and proposed. In dynamic downscaling, regional climate models (RCM) are nested within the coarser-scale GCMs to downscale climatic projections. The major drawbacks of RCM are its complex design and computationally expensive (Hewitson and Crane 1996). In statistical downscaling, a statistical relationship is established between large scale atmospheric variables (predictors) with local (station) scale meteorological variables (predictands) (Harpham and Wilby 2005; Jain et al. 2009). The statistical downscaling approach has shown an advantage over dynamic downscaling as it is faster and simpler in use, and less computationally expensive. Therefore, the Statistical downscaling method becomes a commonly used downscaling tool to determine the future meteorological variables due to climate change at a particular site (Semenov and Barrow 2002; Harpham and Wilby 2005; Smid et al. 2018; Gagnon et al. 2006; Hashmi et al. 2011; Ebrahim et al. 2013; Hassan et al. 2014; Mekonnen and Disse 2018).

In recent years, two widely recognized statistical downscaling tools, namely SDSM and LARS-WG, were applied to fix the problem of mismatch of spatial and temporal scales between large scale features of the GCMs with regional-scale variables. SDSM uses a regression-based method (Wilby and Dawson 2004), whereas LARS-WG is based on a stochastic weather generator (Semenov and Barrow 2002). The methods have been tested in different regions with various climate conditions of the world (Akbari et al. 2015; Daksiya et al. 2017; Ebrahim et al. 2013; Gagnon et al. 2006; Hashmi et al. 2011; Hassan et al. 2014; Mekonnen and Disse 2018; Vallam and Qin 2017). Therefore, the objective of this study is to evaluate and compare SDSM and LARS-WG models in terms of their ability to simulate and forecast rainfall and temperature, which is vital to develop climate change information that can be used for hydrological and overall climate change impact assessment in Tana Basin.

Materials and methods

Study area description

The Amhara National Regional State (ANRS) is located in Ethiopia's north-western and north-central parts (latitude 8°–13°45′ N and 36° and longitude 40°30′ E). According to Central Statistical Agency of Ethiopia (CSA 2008), the region has a total area of around 170,000 km^2 and categorized into 12 administrative zones and 105 woredas with different characteristics of the physical landscape, i.e., valleys, rugged mountains and gorges with elevation ranging from 700 m a.s.l to 4600 m.a.s.l in the eastern and the northwest part, respectively. The Lake Tana basin is the largest sub-basin in the Amhara region, covering an area of 15,096 km^2, including the lake area (Fig. 1). The average annual rainfall and evapotranspiration of the Basin are approximately 1280 mm and 1036 mm, respectively (Allam et al. 2016).

The annual climate is classified into two major seasons, viz. the rainy and the dry season. The rainy season also divided into a minor and major rainy season, which lasts from March to May (*Belg*), and June to September (*kiremt*), respectively, and the dry season, lasts from October to February (*Bega*). As a result of its diverse nature of the region with altitudes ranging from 1327 to 4009 m.a.sl, the Basin contributes national importance because of its high potentials for irrigation development, high-value crops, hydroelectric power development, livestock production, and ecotourism (CSA 2008).

Lake Tana, among one of the Blue Nile River's main source, is Ethiopia's largest lake and the third-largest in the Nile Basin. It is about 84 km long and 66 km wide in the north-western highlands of the country. The lake is one of the natural freshwaters, at an elevation of 1800 m, covering an area of 3000–3600 km^2. Gumera, Ribb, Gilgel Abay, and Megech Rivers are among the main feeding the Lake Tana. These four rivers contribute to the annual water budget of the lake to more than 65% inflow (Setegn et al. 2008). The only surface outflow is the Blue Nile River, measured at the Bahirdar gauge station with an annual flow volume of 4BCM is sourced from Lake Tana.

According to the Abay River Master plan study conducted by BCEOM (1998), land use in the study area is classified as the following: Agriculture covers approximately 51.37%, Agro-pastoral (21.94%), Lake (20.41%), wetland (0.13%), Pastoral (5.47%), Sylvicultural (0.15%), silvopastoral (0.03%) and the urban area covers 0.11%.

Data sources and methods of analysis

Observed data

The Ethiopian meteorological service agency provided basic climatic variables such as daily maximum and minimum temperature and rainfall from 1980 to 2015. To examine the impact of changing climate on basic climatic variables,

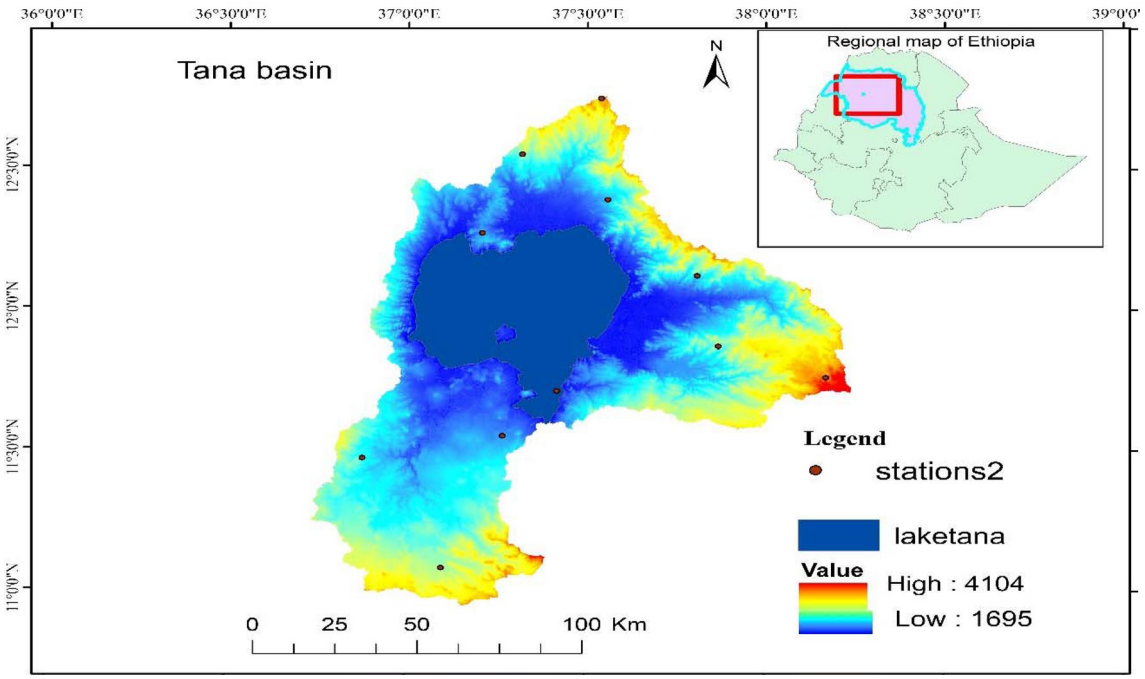

Fig. 1 Spatial distribution of stations

the period from 1980 to 2005 is considered as the reference period, and the period 2011–2100 considered as the future. Hence, in this paper, climate change assessment uses a 36-year reference period to the 95-year future period. Climate modeling data includes rainfall maximum and minimum temperature model output were downscaled and compared with observed datasets obtained from the National Meteorological Agency of Ethiopia for ten stations (Table 1) in Tana basin.

Reanalysis predictor data

Twenty-six daily reanalysis different atmospheric variables obtained from the National Center for Environmental Prediction/National Center for Atmospheric Research (NCEP/NCAR) for the period 1961–2001/2005 for HadCM3/CanESM2 GCMs were used to calibrate and validate SDSM. To downscale the large scale predictor variables of HadCM3 and CanESM2 with emission scenarios (A2, B2, and RCP2.6, RCP4.5 and RCP8.5, respectively) on the period 1961–2099, the validated SDSM was used. The data is usually regraded with a resolution of 2.5° (longitude) by 2.5° (latitude). All scenario data were uniformly regraded to identical resolution with NCEP to reduce Bias due to varying scale.

The model data are provided from both phase three of the Coupled Model InterComparison Project (CMIP3) and phase five of the Coupled Model InterComparison Project (CMIP5). The focus is primarily on evaluating the past performance and projection of future coupled atmosphere–ocean general circulation models (AOGCMs). Therefore, in the study area, the statistically downscaling model (SDSM) and the Long Ashton research station weather generator (LARS-WG) were used to generate future maximum temperature, minimum temperature, and rainfall. Figure 2 shows a schematic diagram of both models.

The reason for selecting the GCMs, specially CanESM2 and HadCM3, was that they are models that made daily predictor variables freely available to be directly fed into SDSM as input, covering the study area with a better resolution. Additionally, Both are widely the most used GCMs of climate change impact studies such as Dibike et al. (2008), Dile et al. (2013), Hassan et al. (2014), Yimer et al. (2009) and Mekonnen and Disse (2018). The NCEP predictor variables of canESM2 and HadCM3 GCM output contains 26 daily predictor variables, and each are listed in Table 2. The required daily meteorological data were collected from the Ethiopian National Meteorological Agency (ENMA) for ten selected stations in the Basin.

Table 1 Detail of stations

No.	Stations	Latitude	Longitude	Altitude	Period
1	Bahir Dar	11°71′	37°50′	1800	1980–2015
2	Gondar	12°63′	37°45′	2133	1980–2015
3	Woreta	11°55′	37°42′	1828	1980–2015
4	DebreTabor	11°86′	38°02′	2706	1980–2015
5	Dangla	11° 25′	36°74′	2122	1980–2015
6	Kemer Dengay	10° 92′	37°25′	2560	1980–2015
7	Injibra	11° 70′	38°43′	2672	1980–2015
8	Wegera	12° 75′	37°63′	2796	1980–2015
9	Addis Zemen	12°12′	37°81′	1815	1980–2015
10	Maksegnet	12° 39′	37°56′	1794	1980–2015

Description of SDSM

The SDSM describes a combination of transfer function-based regression and the stochastic weather generator (Wilby et al. 2004). It performs spatial downscaling using multiple linear regression through daily predictor-predictand relationships to generate local weather condition predictands. The regression-based method is well-known and mostly used downscaling technique (Harpham and Wilby 2005; Wilby et al. 2004). To simulate the present and future projection of meteorological variables using SDSM, daily data corresponds to local predictand (e.g., maximum and minimum temperature and rainfall) and large-scale NCEP/NCAR and GCM of a grid box nearby the stations is required. Wilby et al. 2002 developed an SDSM tool using a combination of stochastic weather generator and multivariate regression method to generate local weather variables from the statistical relationship between large-scale predictors and local climate variables. The following equation gives the relationship between the predictors of large scale and local climate variables as the following:

$$R = F(L) \tag{1}$$

where, R is local climatic variables (predictand), L large scale climate variables (predictor), and F is a deterministic function that empirically estimated from historical observations.

To construct daily local rainfall, maximum and minimum temperature using SDSM, CanESM2 obtained from the Canadian Center for Climate Modelling and Analysis that represents CMIP5 and HadCM3 from United Kingdom Hadley Center that represents CMIP3 were used. Data from the National Center for Environmental Prediction (NCEP) over the period 1961–1990 from its resolution of 2.5° (lat.) × 2.5° (long.) were interpolated to the same grid as HadCM3 of spatial resolution 2.5° (lat.) × 3.75° (long.) and canESM2 2.8125° (lat.) × 2.8125° (long.). The generation of scenarios produced synthetic weather data for

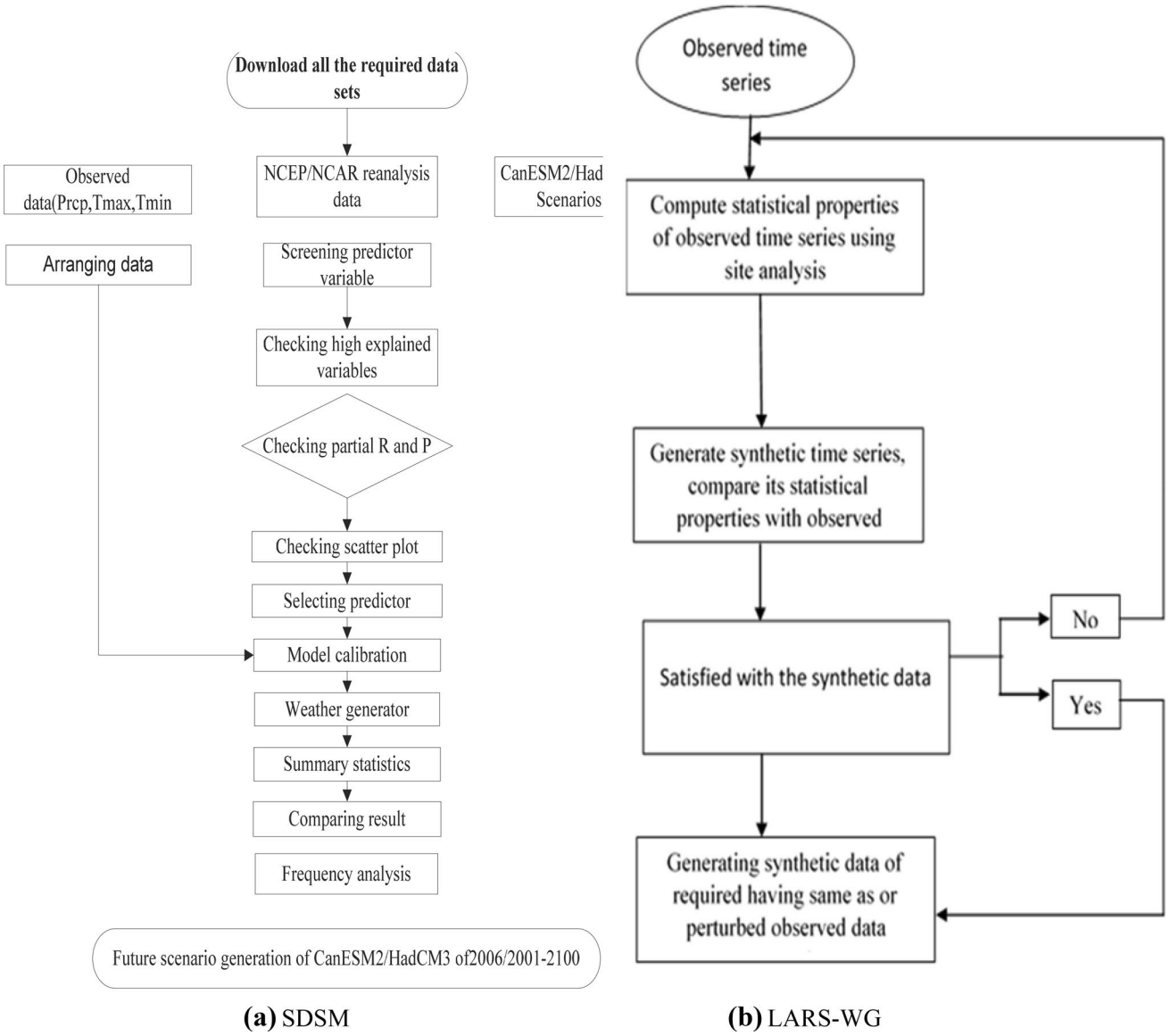

Fig. 2 Diagram of **a** SDSM, **b** LARS-WG

Table 2 HadCM3 and CanESM2 NCEP variables

Variable	Description	Variable	Description
p500	Geopotential height at 500hpa	Prec#	Precipitation
p850	850 hpa Geopotential height	**_f	Airflow strength
s500#	500hpa Specific humidity	**_z	vorticity
s850#	850 hpa Specific humidity	**_u	Zonal velocity
r500*	500 hpa Relative humidity	**_v	Meridional velocity component
r850*	850 hpa Relative humidity	**_zh	Divergence
Temp*	Mean temperature at 2 m	**_th	Wind direction
mslp	Mean sea level pressure	shum	Near surface specific humidity

* Refers predictors variable found only in HadCM3, # indicates predictors only found CanESM2 and ** refers different atmospheric level (p_, p8, p5 represents variables near, 850 hPa height and 500 hpa height, respectively

HadCM3 A2 and B2 scenarios from the year 1961 to 2099 and for CanESM2 RCP2.6, RCP4.5 and RCP8.5 scenarios from the year 2011–2100 were projected.

The downscaling procedure for the SDSM model follows a series of discrete processes given by (Wilby et al. 2004; Wilby and Dawson 2013) (1) pre-screening possible predictor variable (2) calibration of the model and determine the parameters (3) weather generation, generating of synthetic daily weather series based on the given predictor variables (4) future ensemble data generated using the predictor variables from the GCM (5) analysis and compare both observed and downscaled data using statistical characteristics. The most critical stage in the statistical downscaling process is to screen the significant predictor variables for model calibration. It is a fundamental level to develop statistical downscaling models. Therefore, the success of the statistical downscaling model using SDSM is primarily determined by the selection of suitable predictor variables (Wilby et al. 2004).

To build downscaled data from the given predictand and selected predictor variables on the multiple regression equations, SDSM model calibration was used. The model was structured as daily and monthly rainfall, maximum and minimum temperature downscaling. Adjustment of modeled data to reflect the observed data using bias correction was carried out. The weather generator makes ideal use of independent data to validate the calibrated model. This operation generates synthetic daily weather data sets for the given time together with a parameter file prepared during model calibration using regression model weights. Finally, SDSM provides a summary with statistics function to compare the observed and simulated data function that summarizes the observed and simulated data results. In this climate change study, for the pre-screening purpose, all twenty-six large-scale predictor variables from the National Center for Environmental Prediction (NCEP) were used. For model calibration and validation between predictor and predictand data in SDSM, the period was divided into two; from 1980 to 1995/1980 to 2000 for calibration and 1996–2001/1996–2005 for validation of HadCM3/CanESM2 GCMs, respectively were used. Following validation and summary statistics, the model used to generate future three-time slice predictions as 2030 (2011–2040), 2050 (2041–2070), and 2080 (2071–2100) with scenarios available for each GCM. Rainfall and temperature change of future trends for a given time slice are calculated as the following.

$$\Delta P = \frac{(Sm.P - Obs.P) \times 100}{Obs.P} \tag{2}$$

$$\Delta T = Sm.T - Obs.T \tag{3}$$

where, $Sm.P$ and $Sm.T$ indicate simulated precipitation and temperature, respectively. $Obs.P$ and $Obs.T$ indicates observed precipitation and temperature, respectively.

Description of LARS-WG

LARS-WG is a stochastic weather generator based on a series approach to weather data simulation under the current and future climate conditions (Semenov and Barrow 2002, 1997). It can produce synthetic daily rainfall, maximum temperature, minimum temperature, and solar radiation for a single site (Giorgi et al. 2009; Semenov and Barrow 1997). In this study, to generate simulated weather data corresponding to observed data, four GCMs (HadCM3, GFCM21, NCCCS, and MPEH5) with the available emission scenario were used. The weather generator needs the required meteorological variable in the form of a daily time series. As a result, empirical distribution is developed by LARS-WG to simulate dry and wet spell length, daily rainfall (mm), minimum and maximum temperature (°C), and solar radiation (MJ/m^2/day) (Hassan and Harun 2011; Semenov and Barrow 2002).

The statistical parameter is used to simulate synthetic climate data ensembles from the historical input record. Input data of the LARS-WG model are a series of daily observed data (rainfall, minimum temperature, and maximum temperature) of the base period (1980–2010). To adjust future climatic variables under selected Representative Concentration Pathway (RCP), the modified data calculated from the baseline period (1980–2010), which are adjusted by the change factor, was used. The monthly change was computed as relative change and absolute change for rainfall and temperature, respectively (Semenov and Barrow 2002, 1997). The model performs three main steps through calibration, validation, and generation of climate scenarios. Synthetic weather data corresponding to observed data are generated during the calibration process. Following calibration, weather generator performance was computed by comparing the mean and standard deviation between observed and simulated data. Finally, future climatic variables using LARS-WG from HadCM3, GFCM21, NCCCS, and MPEH5 GCMs with the common A2, B1, and A1B scenarios were generated with the 2030 s, 2050 s, and 2080 s period.

Model performance evaluation metrics

During the calibration and validation of the downscaling model on time series, a simulation of mean daily and monthly rainfall, maximum and minimum temperature was checked using the coefficient of determination (R^2), root mean square error (RMSE), Nash–Sutcliffe efficiency (NSE), and Bias(B) defined as;

The coefficient of determination (R^2) is essential to make a comparison between the explained variance of modeled data with the total variance of the observed data

$$R^2 = \frac{\sum_{i=1}^{n}(y_i - \bar{x})^2}{\sum_{i=1}^{n}(x_i - \bar{x})^2} \quad (4)$$

RMSE is described as the difference between simulated and observed values. The mathematical representation is given:

$$\text{RMSE} = \sqrt{\frac{\sum_{i=1}^{n}(x_i - y_i)^2}{n}} \quad (5)$$

NSE determines the relative magnitude of the variance of residues and measured data, which ranges from $-\infty$ to 1. It gives as:

$$\text{NSE} = 1 - \frac{\sum_{i=1}^{n}(x_i - y_i)^2}{\sum_{i=1}^{n}(x_i - \bar{x})^2} \quad (6)$$

$$\text{Bias} = \frac{\sum_{i=1}^{n} x_i}{n} - \frac{\sum_{i=1}^{n} y_i}{n} \quad (7)$$

where X_i is th observed data, Y_i is the simulated data.

Besides, statistical tests, namely equally weighing metrics and varying weighing metrics using metrics of MAE, RMSE, and Bias, were computed for model performance comparison. These methods are the most widely acceptable numerical metrics to evaluate the comparative performance of downscaling models on the basis of long term monthly average precipitation (Goly et al. 2014; Hashmi et al. 2011; Singh and Goyal 2016). Measures such as the coefficient of determination and coefficient of efficiency are not included due to oversensitive to extreme values of the measures. The following are steps applied for the equally weighted: (i) comparing performance metric values among the models and ranking for every station. The value 1 gives for the model that shows smaller value, value 2 gives for the middle between, and the value 3 provides the model that has a larger value. (ii) Summing up each model score across all the stations. (iii) The model is ranked based on the total score, the model has smaller total metrics score 1, and the model has larger total metrics scores 3.

The varying weights technique was applied and calculated as Eq. (8) (Goly et al. 2014). In this case, the metrics are arranged and giving the value to MAE, RMSE and % Bias (0.45, 0.4 and 0.15, respectively)

$$W_i = W_{\text{MAE}}\frac{\text{MAE}_i}{\text{MAE}_{\max}} + W_{\text{RMSE}}\frac{\text{RMSE}_i}{\text{RMSE}_{\max}} + W_{\text{Bias}}\frac{\text{Bias}_i}{\text{Bias}_{\max}} \quad (8)$$

where W_i refers to overall performance measure, and $0 \le W_i \le i$ refers to a downscaling model.

Results and discussion

Predictor variables selection

The success of the SDSM-based downscaling approach depends on the choice of predictor variables. Developing predictand–predictor relationship is one of the first influential steps in statistical downscaling procedures. Screening of potential predictors was performed on the basis of a correlation matrix between each predictand and the National Centers for Environmental Prediction (NCEP) predictor variables. Daily data comprising 26 large-scale predictor variables derived from NCEP reanalysis (Table 2) were used, and the predictors of a high correlation coefficient with the predictand were selected for all stations and the potential predictor (summarized in Fig. 3). In each station,

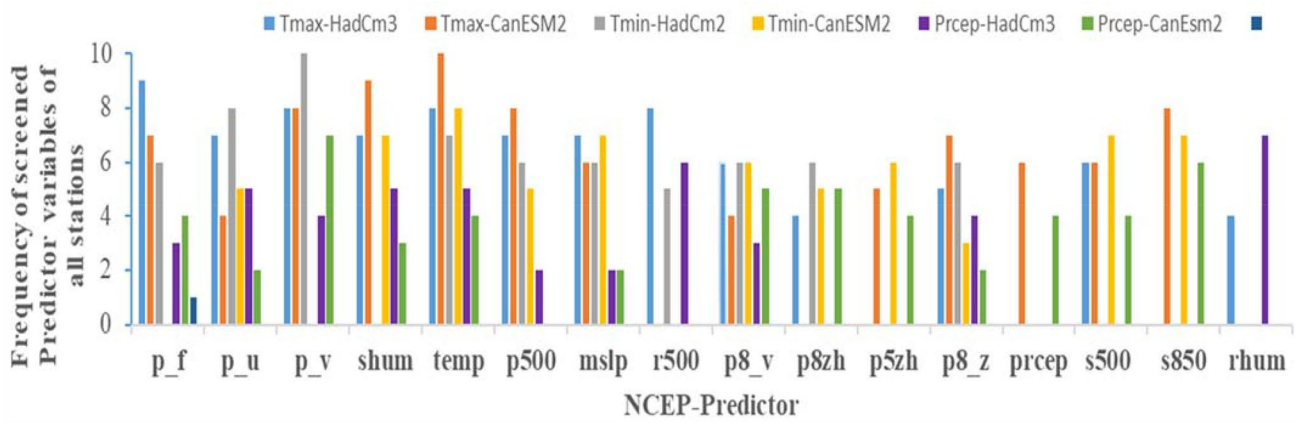

Fig. 3 Screened variables of NCEP predictors of the two GCMs for observed rainfall, T_{max} and T_{min}

the predictor was selected based on the highest correlation with the observed predictand (T_{max}, T_{min}, and rainfall). For instance, the set of p_f, p_v, shum, temp r500, and s850 was a dominant predictor variable of temperature, and rhum, r_500, s_850, p8_v, and p_v performed well to predict rainfall in the study area. This indicates that each predictor variable identified for each GCM controlled different local variables of each station. Even if a predictor variable did not give good correlations with the predictand in some stations, it was still selected as a potential predictor variable in the other stations, particularly for rainfall as it describes the conditional process. On the other hand, as temperature is not a conditional process, the selection of predictor variable for rainfall was not difficult. As described in Fig. 3, mean temperature at 2 m (temp) became a potential predictor of temperature (T_{max} and T_{min}), covering almost all of the 10 stations of the study area. This variable was expected to generate future maximum and minimum temperature scenarios as it is believed to be related to temperature (Gulacha and Mulungu 2017; Harpham and Wilby 2005; Hasan et al. 2017; Hessami et al. 2008; King et al. 2012; Maraun et al. 2010; Wilby and Dawson 2013). Before running the SDSM to effectively downscale the future climate conditions with GCM outputs, it was necessary to calibrate the relationship between observed and simulated climate variables (rainfall, T_{max} and T_{min}). In this study, calibration periods of 15 and 20 years (1980–1995/2000) of baseline for HadCM3/CanESM2 GCMs, respectively, were used. Following calibration, the 5-year and 10-year data (1996–2001/2005) were used for validation in all stations of HadCM3/CanESM2 GCMs, respectively.

Calibration and validation of SDSM and LARS-WG

A simulation of daily and monthly rainfall, T_{max} and T_{min}, of SDSM and LARS-WG results was compared and checked with observations during the calibration and validation period using graphical representation and statistical parameters, namely, coefficient of determination (R^2), root mean square error (RMSE), and Nash–Sutcliffe efficiency. Table 3 shows statistical comparison between observed and simulated T_{max}, T_{min}, and rainfall during the calibration and validation period under SDSM and LARS-WG models.

The graphical and statistical comparison of rainfall, T_{max} and T_{min} using SDSM and LARS-WG was run to examine the performance of the model as shown in Fig. 4 and Table 3 (average for all stations). Overall results indicated acceptable response of the model evaluated by different statistical performance indicators under HadCM3 and CanESM2 GCMs. With regard to model comparison, both SDSM and LARS-WG were not able to capture good daily rainfall data series but were able to capture fairly good monthly rainfall data series. However, the difference in average of observed and simulated daily rainfall by SDSM over the stations was 0.5–0.7 mm/day and 5.7–9.5 mm/month for the CanEMS2 and HadCM3 models, respectively. A slightly small difference in average rainfall over the stations was recorded by LARS-WG of HadCM3GCM, with 0.48 mm/day and 5.5 mm/month (Table 4).

Even though the LARS-WG showed a small difference between observed and simulated rainfall and less RMSE value than SDSM HadCM3 models, evaluation metrics of the RMSE value revealed that SDSM/CanESM2 performed best in simulating the long-term mean rainfall in both equally weighted and varying weight metrics (Tables 6 and 7). Overall, the result proved an excellent performance of SDSM and LARS-WG in modeling T_{max} and T_{min} than rainfall during calibration and validation as the value of R^2 is higher for temperature than rainfall. This may be due to the spatially nonconservative nature of precipitation (Gagnon et al. 2006). The result is in line with previous studies(Hassan et al. 2014; Huang et al. 2011; Liu et al. 2011), which indicated a good performance of SDSM and LARS-WG for simulating T_{max} and T_{min} than rainfall.

It can be observed from the results that low RMSE and high R^2 were found for T_{min} (RMSE < 0.51 with SDSM, < 0.7 with LARS-WG and R^2 of 0.87–0.98 with SDSM, 0.76–0.91 with LARS-WG) and T_{max} (RMSE ≤ 0.52 with SDSM, ≤ 0.61 with LARS-WG and R^2 of 0.85–0.97 with SDSM and 0.77–0.84 with LARS-WG) in the HadCM3 model. However, the maximum R^2 value was obtained during the monthly calibration period for T_{max} (0.97) and T_{min} (0.98) under CanESM2 of SDSM. Table 3 and Fig. 4 indicate the models are well-validated, but the accuracy is less compared to the calibration result, and the CanESM2 model was able to perform better than the HadCM3 GCMs simulated by both SDSM and LARS-WG models regarding all climatic variables (rainfall, T_{max} and T_{min}).

Future climate variables downscaling

Downscaling with SDSM

After calibration and validation of both SDSM and LARS-WG, the next step was to downscale the future temperature and rainfall using the HadCM3 and CanESM2 in various scenarios. The downscaled average annual rainfall maximum and minimum temperatures using the Thiessen polygon method calculated from all stations is presented in Fig. 5. The results from all models under three time slices (2030 s, 2050 s, and 2080 s) indicate that rainfall will increase until 2100.

The minimum and maximum change of mean annual rainfall are predicted between 9.9% (2030) and 44.7% (2080) under the HadCM3B2 and CanESM2 RCP8.5 scenarios, respectively, compared with the baseline period (Fig. 5).

Table 3 Statistical performance of the models (SDSM and LARS-WG) with HadCM3 and CanESM2GCMs

	RMSE			R^2			NSE			Bias		
	SDSM*	SDSM$	LARS-WG	SDSM*	SDSM$	LARS-WG	SDSM*	SDSM$	LARS-WG	SDSM$	SDSM*	LARS-WG
Rainfall												
Calibration(daily)	8.6	5.8	6.3	0.52	0.71	0.64	0.63	0.52	0.68	0.84	2.1	0.63
Calibration (monthly)	11.1	6.9	8.4	0.57	0.76	0.55	0.85	0.76	0.71	1.72	2.7	2.3
Validation(daily)	2.8	6.8	3.9	0.55	0.68	0.70	0.37	0.62	0.56	1.11	1.1	0.80
Validation(monthly)	18.1	11.3	15.2	0.61	0.64	0.77	0.77	0.84	0.81	3.2	2.3	3.4
Minimum temperature												
Calibration(daily)	0.21	0.34	0.52	0.91	0.92	0.90	0.88	0.9	0.76	0.07	0.7	0.93
Calibration (monthly)	0.36	0.28	0.70	0.95	0.98	0.91	0.94	0.92	0.88	0.02	0.4	0.57
Validation(daily)	0.47	0.36	0.41	0.87	0.88	0.76	0.71	0.88	0.82	0.32	0.69	0.6
Validation(monthly)	0.51	0.46	0.62	0.93	0.94	0.88	0.92	0.94	0.84	0.64	0.5	0.78
Maximum temperature												
Calibration(daily)	0.2	0.28	0.43	0.96	0.88	0.84	0.77	0.89	0.72	-0.45	0.5	1.1
Calibration (monthly)	0.4	0.40	0.52	0.93	0.97	0.79	0.86	0.91	0.74	-0.61	0.9	0.82
Validation(daily)	0.3	0.25	0.42	0.87	0.94	0.77	0.79	0.86	0.82	-0.27	0.7	0.87
Validation(monthly)	0.4	0.32	0.61	0.89	0.93	0.78	0.91	0.88	0.86	-0.33	0.7	0.1.3

*Refers HadCM3 and $ refers Can ESM

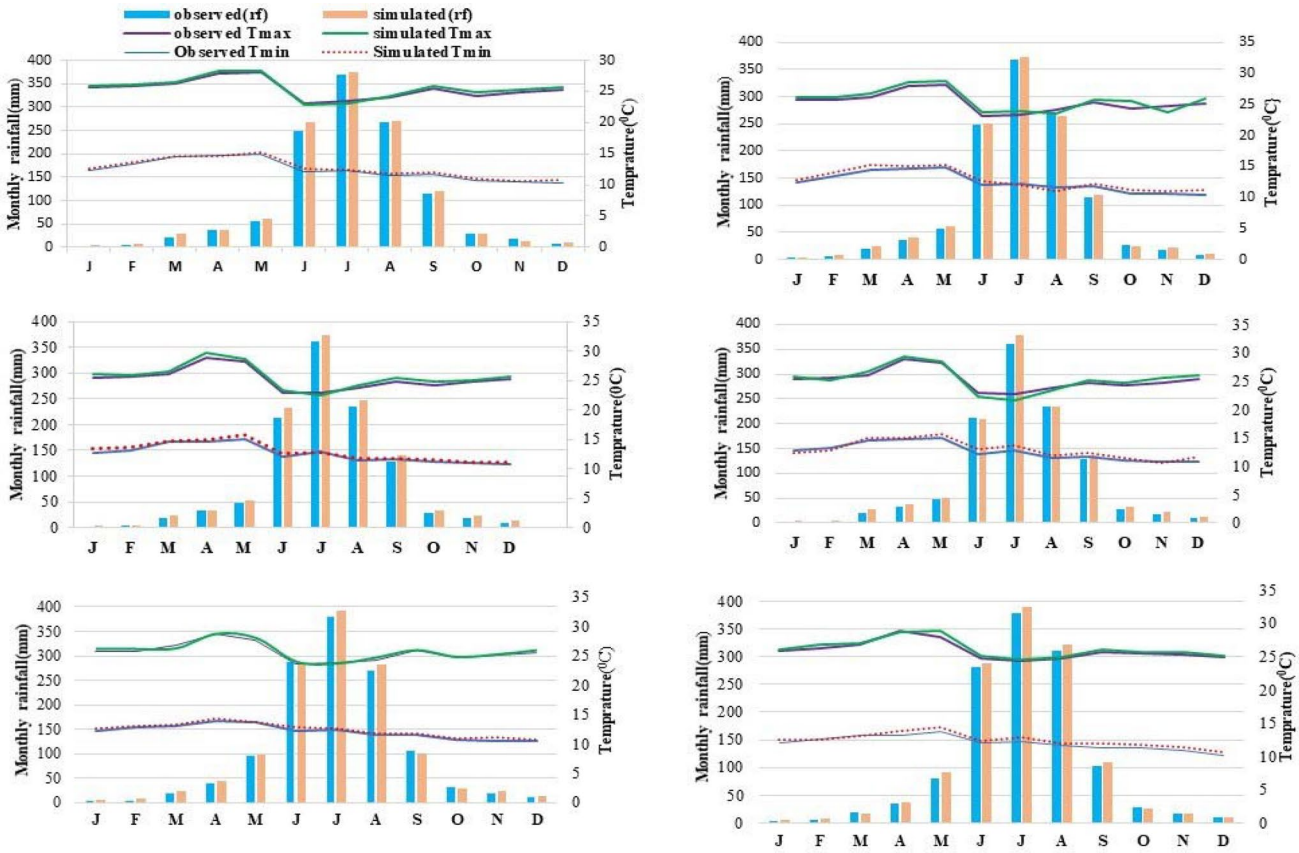

Fig. 4 Calibration and validation result of mean monthly rainfall and temperature. Top left and right calibration with SDSM and LARS-WG, respectively, middle left and right, validation with SDSM and LARS-WG, respectively, using HadCM3, and bottom left and right indicated calibration and validation result of SDSM using CanESM2

The maximum and minimum annual rainfall change in 2050 is projected to be 31.4% and 11.6% under the RCP8.5 and B2 scenarios of CanESM2 and HadCM3, respectively. On the other hand, the B2 scenario showed a minimum change of rainfall over the study area. Similar to annual r change, the maximum change of annual Tmax occurred on the time slice of 2080 under RCP8.5 whereas minimum change was observed on the time slice of 2050 under RCP2.6. The downscaled result also revealed that, except for RCP2.6 of 2030 and 2050, the minimum temperature change generated by the CanESM2/HadCM3 GCMs was less than the change of maximum temperature all time periods across the study area (Fig. 5). The result is in line with studies carried out in different parts of Ethiopia that indicated the highest increasing range of maximum temperature than minimum temperature (Ayalew et al. 2012; Feyissa et al. 2018).

Table 4 Mean observed and simulated rainfall, T_{max} and T_{min} of the baseline period

	SDSM		LARS-WG
	HadCM3	Can ESM2	HadCM3
Daily rainfall (mm)			
Observed	6.8	6.9	6.8
Simulated	7.5	7.4	7.28
Monthly rainfall (mm)			
Observed	119.1	120.4	119.1
Simulated	128.6	126.1	124.6
Max temperature (°C)			
Observed	25.91	25.99	25.98
Simulated	26.01	25.84	26.21
Min temperature (°C)			
Observed	12.01	12.13	12.01
Simulated	12.24	12.26	12.36

Figures 6, 7 and 8 present the future percentage change of mean monthly rainfall and T_{max} and T_{min} of the study area on the time slices of the 2030 s, 2050 s, and 2080 s with reference to a baseline period under HadCM3/CanESM2 with the available scenarios, respectively. The monthly basis result indicates that rainfall decreases in both January and February under RCP4.5 and RCP8.5 and that monthly rainfall also decreases in the month of March as reported by RCP2.4 of CanESM2 GCM, whereas both

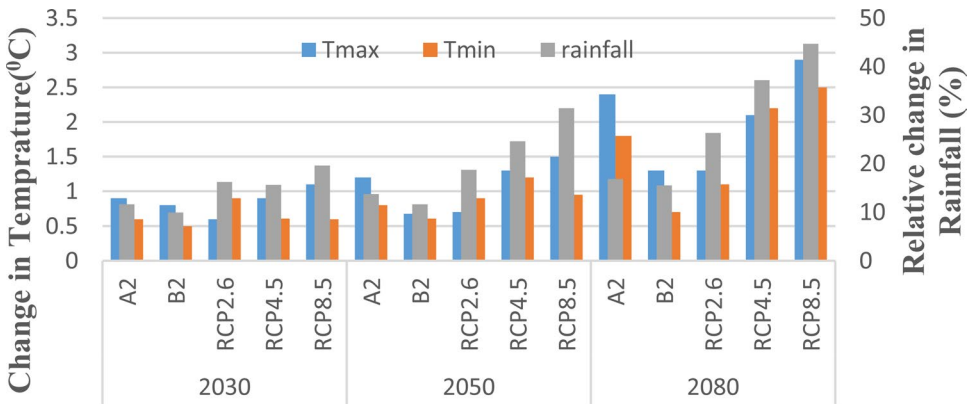

Fig. 5 HadCM3 and CanESM2 GCMs relative changes of mean annual rainfall, change of mean annual T_{max} and T_{min} down-scaled by SDSM

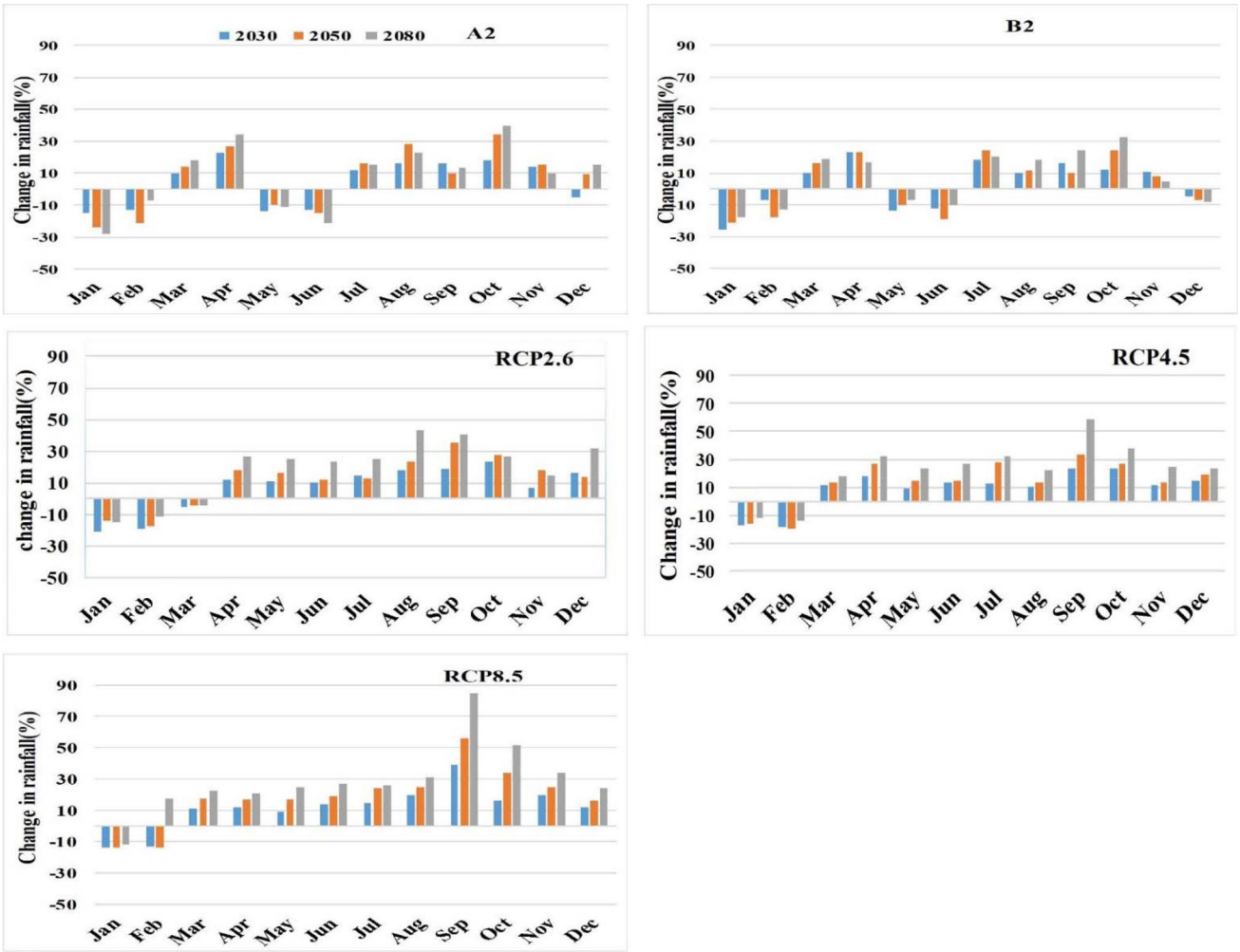

Fig. 6 Relative change of mean monthly rainfall (SDSM)

increasing and decreasing trends of mean monthly rainfall were observed on both scenarios of HadCM3 GCM. In general, RCP8.5 of CanESM2 indicates a more noticeable change of mean annual temperature than do RCP2.4 and RCP4.5 on all-time slices.

The future rainfall change on a monthly basis was revealed to increase by 84.5% and 58.4% in September 2080 under RCP8.5 and RCP4.5 of CanESM2, respectively. The result also indicates a relatively small monthly rainfall change occurred on HadCM3 GCM compared with

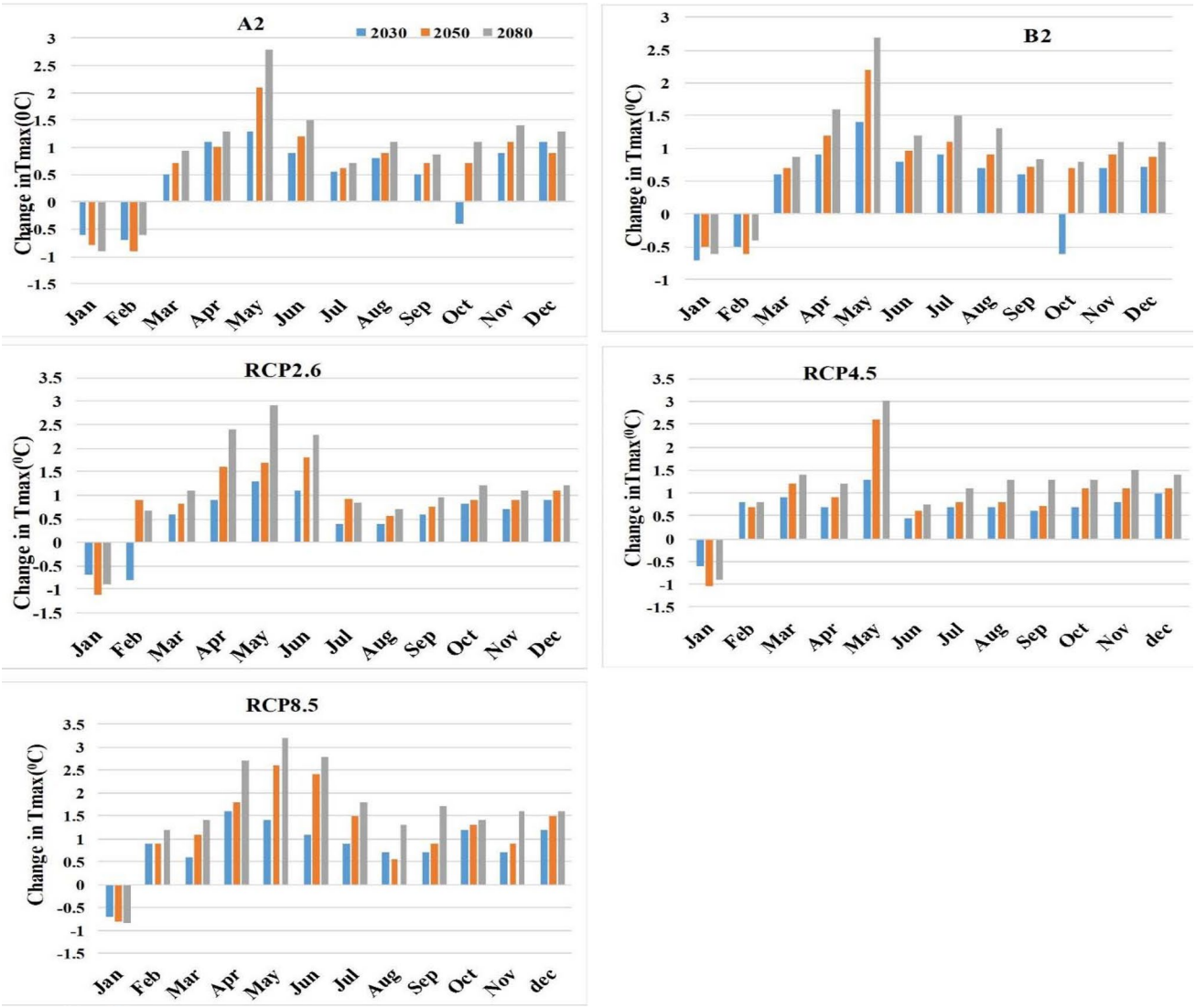

Fig. 7 Change of maximum temperature (SDSM)

CanESM2, with a maximum value of 39.6% in October 2080 under the A2 scenario. In contrast, the maximum reduction of rainfall was observed in January 2030 under the B2 scenario of HadCM3 GCM. Generally, the range of monthly rainfall change has shown to vary between − 14% and 79%, − 19% and 84.5%, and − 21% and 46% under RCP8.5, RCP4.5, and RCP2.6 of CanESM2, respectively.

The highest positive change of monthly T_{max} was observed in May 2080 (3.2 °C under RCP8.5) and (3.0 °C under RCP4.5), whereas the lowest positive change of T_{max} was observed in both July and August (0.4 °C) of 2030 under RCP2.6 of CanESM2. Conversely, except for RCP8.5 of 2030, the change of T_{min} was projected to be highest in June on both GCMs of all periods. The maximum change of T_{min} was projected to be 2.7 °C in June 2080 under RCP8.5. The maximum reduction (− 0.9 °C) of the mean monthly change of T_{max} was observed in January 2050 under the B2 scenario of HadCM3 GCM. In general, the RCP8.5 scenario shows a noticeable future increase of rainfall and temperature over the study area in all three time periods.

Downscaling with LARS-WG

Similar to SDSM, the analysis of climate downscaling using LARS-WG was done by classifying future data by three time windows (viz., 2011–2040, 2041–2070, and 2071–2100 as 2030 s, 2050 s, and 2080 s, respectively). The results of rainfall prediction using the four GCMs and their ensemble under three scenarios (A1B, B1, and A2) are presented in Table 5. Relative change in rainfall results revealed that the three of the GCMs indicated a clear increasing trend of mean annual rainfall over the basin. On the other hand, GFCM21

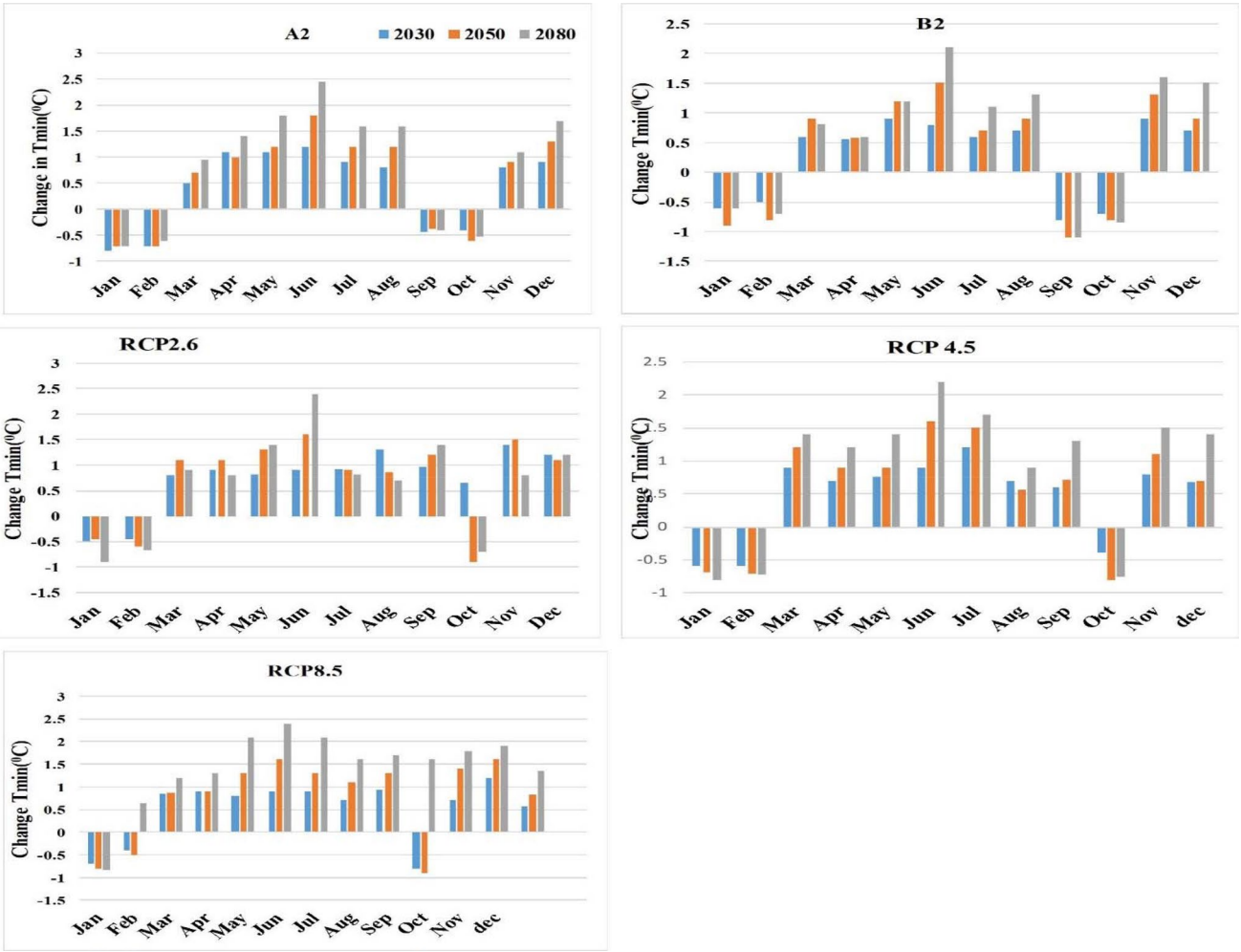

Fig. 8 Change in minimum temperature (SDSM)

GCM was found to have unstable results in the direction and magnitude of mean annual rainfall, particularly for the 2030 and 2080 time periods. An increase of mean annual rainfall was shown on the other three GCMs with a maximum rise by MPEH5 GCM, while the highest reduction was registered by GFCM21 (Table 5). The A1B scenario of MPEH5 showed a maximum relative change of mean annual rainfall during 2030, while the A2 scenario indicated a maximum change in 2050 and 2080. Relative change of mean annual rainfall during the 2030 s is projected between − 3.9% and 9.8% for the A1B, − 3.4% and 8.4% for the B1, and − 3.2% and 13.4% for the A2 scenario. The relative change of mean annual rainfall in the 2050 s was projected between − 14.8% and 17.2%, − 9.6% and 21.4%, and − 2.6 and 22.6%, and in the 2080 s the relative change of rainfall may project between − 6.1% and 24.3, − 4.3% and 29%, and 16% and 45.2% under the A1B, B1, and A2 scenarios, respectively. However, such increasing trends are not obvious in the case of mean monthly rainfall. The mean monthly rainfall of HadCM3 (during December and November) and MPEH5 (during December) on all scenarios showed a decreasing relative change of rainfall. In general, the relative change of annual rainfall obtained from the model average showed an increasing trend of rainfall between 3.9% and 18.6%, which also showed the closest result with HadCM3 GCM (4.2% and 19.2%) as shown in Table 5.

T_{max} calculated from the ensemble mean shows a result consistent with that of HadCM3 GCM (A2 and A1B scenarios) and MPEH5 GCM (A2 scenario) in all three time periods of the future. Similar to T_{max}, the change of mean annual T_{min} is also projecting an increase by 4.2 °C, 2.3 °C, and 1.8 °C under the A1B, A2, and A2 scenarios by 2080, 2050, and 2030, respectively. The HadCM3 A2 scenario showed the closest result to the ensemble mean in all three time periods of the future. This indicates that from the selected CMIP3 GCMs, HadCM3 performed better to represent local climatic variables, which is in agreement with previous studies in the study area and different parts of Ethiopia (Dile

Table 5 The six GCMs Relative change of mean annual rainfall, change in maximum and minimum temperature downscaled by LARS-WG

GCM/scenario	Observed	2030			2050			2080		
	1215 (mm)	A1B	B1	A2	A1B	B1	A2	A1B	B1	A2
Mean annual rainfall (%)										
GFCM21		4.1	-3.4	-3.2	-14.8	-9.6	-2.6	-6.1	-4.3	16
HadCM3		7.2	4.1	13.1	8.2	10.8	15.3	14.8	17.2	19.2
MPEH5		9.8	7.6	8.4	17.2	21.4	22.6	23.4	29	45.2
NCCCS		3.9	8.4	9.3	13.2	16.6	18.6	24.3	26.7	28.6
Model average		6.8	3.9	12.7	10.3	11.3	17.6	15.8	18.0	18.8
Mean T_{max} (°C)	25.3 (°C)									
GFCM21		0.4	0.3	0.6	1.1	1.4	1.5	2.6	2.2	2.2
HadCM3		0.6	0.5	0.7	1.7	1.8	1.9	3.8	3.2	3.5
MPEH5		0.6	0.5	0.70	1.8	2	2.1	4	3.5	3.9
NCCCS		0.8	0.7	0.95	1.9	2.1	2.4	4.6	4.1	4.1
Model average		0.6	0.6	0.80	1.7	1.9	2	3.7	3.2	3.6
Mean T_{min} (°C)	14.1 (°C)									
GFCM21		0.4	0.3	0.4	0.9	1.1	1.3	2.5	1.8	2.2
HadCM3		0.5	0.4	0.6	1.4	1.5	1.8	3.5	3.3	3.3
MPEH5		0.5	0.6	0.6	1.6	1.9	2.1	3.8	3.7	3.8
NCCCS		0.7	0.6	0.7	1.8	1.6	2.4	4.3	3.1	3.9
Model average		0.5	0.5	0.6	1.5	1.4	2	3.4	3.2	3.2

et al. 2013; Feyissa et al. 2018; Mekonnen and Disse 2018). Generally, the results showed that the maximum increase is projected by NCCCS GCM (4.6 °C and 4.2 °C) and the minimum increase by GFCM 21 (0.3 °C) for both T_{max} and T_{min}, respectively.

Comparison of SDSM and LARS-WG results

As a result of differences in their downscaling strategy and basic concepts, the future result of the two models may show a different output with the same observed input data. SDSM uses changes in atmospheric circulation models in terms of large-scale predictors, which can be considered more reliable. LARS-WG, on the other hand, uses relative change factors that derive from the direct climatic variable production of a GCM (Chen et al. 2011; Harpham and Wilby 2005). Therefore, in this study, the emphasis has been given to the comparative performance evaluation of the two downscaling methods with several statistical metrics and graphical tests. In addition to the statistical performance evaluation methods described above, equally-weighted score and varying weighted score methods were evaluated and ranked at each site shown in Table 6 for RMSE, and the same was done for other metrics described as Fig. 7.

Table 6 Performance and ranking of the models during the baseline period for RMSE performance metrics

Stations	RMSE			Equally weighted score			Varying weights score		
	SDSM/ CanESM2	SDSM/ HadCM3	LARS-WG	SDSM/ CanESM2	SDSM/ HadCM3	LARS-WG	SDSM/ CanESM2	SDSM/ HadCM3	LARS-WG
Addis Zemen	7.2	14.7	17.3	1	2	3	0.16	0.33	0.40
Bahir Dar	8.2	10.9	8.8	1	3	2	0.37	0.4	0.32
Gondar	8.7	18.6	11.7	1	3	2	0.18	0.40	0.25
Maksegnet	12.7	9.4	16.3	2	1	3	0.31	0.23	0.40
Woreta	14.8	23.8	9.4	2	3	1	0.25	0.40	0.16
DebreTabor	11.3	18.1	14.4	1	3	2	0.25	0.40	0.32
Dangla	8.9	23.3	10.2	1	3	2	0.15	0.40	0.18
Kemer Dengay	13.8	24.3	13.1	2	3	1	0.22	0.40	0.22
Injibra	16.7	14.6	13.6	3	2	1	0.4	0.35	0.33
Wegera	12.8	23.3	16.2	1	3	2	0.21	0.40	0.28
Overall score			15		26	19	2.5	3.71	2.85

The scores for each model were summed up and ranked accordingly as presented in Table 7. The results show that CanESM2 of SDSM performed best in simulating long-term average values in both evaluation metrics. For the comparison of the two statistical downscaling methods (SDSM and LARS-WG), the A2 scenario of HadCM3 GCM was used with both the LARS-WG and SDSM methods to test how the GCM results were influenced by the different downscaling method with the same forcing scenario. The results obtained from the two downscaling methods were found to be comparable, and generally increasing trends in rainfall, T_{max} and T_{min} was shown on both methods. However, the magnitude of future change in climatic variables downscaled by the two methods, as presented in Fig. 9 indicates that LARS-WG over predicts rainfall (for all the periods) and temperature (for 2050 and 2080) compared with SDSM. The relative change associated with mean annual rainfall using LARS-WG is about 19.2%, and the average increase in mean annual T_{max} and T_{min} is about 3.5 °C and 3.3 °C, respectively, in the 2080 s. Conversely, changes in mean annual rainfall, T_{max} and T_{min} predicted by SDSM with the same period were about 16.5%, 2.4 °C, and 1.8 °C, respectively. Hence this contrasting future implication behind the two models is the result of the differences in their downscaling strategy and basic concepts as described above.

Therefore, more caution is required to downscale rainfall through LARS-WG as it is not very reliable in simulating by GCMs due to GCM-induced output error, which will propagate the error of downscaling (Dibike and Coulibaly 2005). The good performance of CanEsm2 downscaled by the SDSM model shows a better agreement with previous studies conducted in Ethiopia (Ebrahim et al. 2013; Mekonnen and Disse 2018).

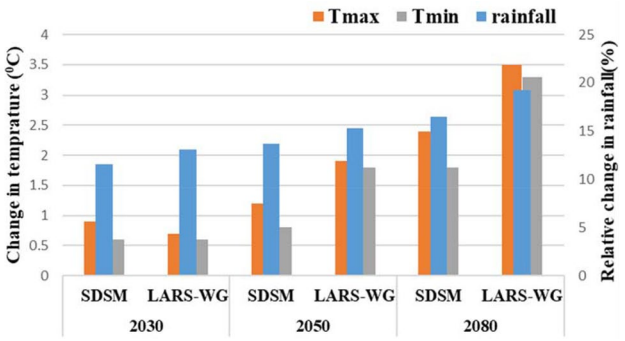

Fig. 9 HadCM3 GCMs relative change of mean annual rainfall, change in maximum and minimum temperature with the common A2 scenario of SDSM and LARS-WG for three time periods of the study area

Conclusions

Climate models and method of downscaling are among many factors linked with the simulation of future climate-change-related uncertainty analysis. In this climate change study, a multimodal approach based on different GCMs was employed, particularly focused on two well-established statistical downscaling methods, SDSM and LARS-WG. The performance of the models was evaluated in terms of their ability to simulate current and downscale the future rainfall and temperature. The comparative analysis using different statistical measures between the two models with the given GCMs indicates that CanESM2 GCM by SDSM performs very well at most of the stations and ranks first of the others for all climatic variables. This may be due to the fact that increasing performance of models across the generations since IPCC AR5 developed a new set of radiative forcing scenarios that replaced the special report of emission scenarios. Large intermodal differences were shown downscaled from the four GCMs used in LARS-WG. One GCM reported that future rainfall will decrease whereas three GCMs indicated a future increase of rainfall in all three time windows. The model average from LARS-WG and the individual model result from SDSM showed a general increasing trend for all three climatic variables (rainfall, T_{max} and T_{min}) in all three time periods (2030,2050 and 2080).

The SDSM, particularly with CanESM2 GCM, approximates the observed climate data series corresponding to the present climate series reasonably well and performs well to downscale T_{max} and T_{min} during the calibration and

Table 7 Ranking of downscaling models for statistical measures (RMSE, MAE, and Bias) during the baseline period

Equally weighted overall score				Varying weights overall score			
Metrics	SDSM/ CanEsm2	SDSM/ HadCM3	LARSWG	Weight	SDSM/ CanEsm2	SDSM/HadCM3	LARS-WG
RMSE	15	26	19	0.4	2.5	3.71	2.85
MAE	14	24	16	0.45	3.1	4.91	3.31
Bias	12	18	13	0.15	1.13	1.50	1.24
Total	41	68	48	1.0	6.73	10.12	7.4
Rank	1	3	2		1	3	2

The numbers in the table show the total ranking scores average from 10 stations

validation periods in contrast to LARS-WG. Even though the A2 scenario of HadCM3 GCM was used by the two models in common, the downscaled rainfall and temperature were not the same. There was a relatively small change of T_{max} and T_{min} during the 2050 s and 2080 s and of annual rainfall during all time windows as compared with LARS-WG. It can be concluded from the downscaled results that all the stations in the study area will face higher rainfall and hotter temperatures compared to the current climate. This change of future rainfall can be a good advantage for rain-fed and irrigation agriculture to maximize agricultural production. Conversely, the maximum positive rainfall change may occur during a major rainy season (April–July), when about 70% of annual rainfall occurs, which could pose a potential threat of flood and related hazards. In general, this study has shown that future climate change will likely occur that may change the hydrology of the study area. On the basis of the results obtained in this study, the CMIP5 model (CanESM2) can simulate the present and project the future better than the CMIP3 (HadCM3 and others) GCMs. Both SDSM and LARS-WG models can be adopted for future climate change impact assessment studies with reasonable confidence. However, the climate data downscaled using the two methods indicates that LARS-WG projected a relatively higher increase range than the SDSM. Therefore, SDSM is more preferred to asses climate change related studies in the study area.

References

Akbari H, Rakhshandehroo GR, Afrooz AH, Pourtouiserkani A (2015) Climate change impact on intensity-duration-frequency curves in Chenar-Rahdar River basin. Watershed Manag 2015(September):48–61. https://doi.org/10.1061/9780784479322.005

Allam M, Jain A, McLaughlin D, Eltahir E (2016) Estimation of evaporation over the upper Blue Nile basin by combining observations from satellites and river flow gauges. Water Resour Res 52(2):644–659

Anyah RO, Qiu W (2012) Characteristic 20th and 21st century precipitation and temperature patterns and changes over the Greater Horn of Africa. Int J Climatol 32(3):347–363. https://doi.org/10.1002/joc.2270

Ayalew D, Tesfaye K, Mamo G, Yitaferu B, Bayu W (2012) Outlook of future climate in north-western Ethiopia. Agric Sci 3(4):608–624

Beecham S, Rashid M, Chowdhury RK (2014) Statistical downscaling of multi-site daily rainfall in a South Australian catchment using a generalized linear model. Int J Climatol 34(14):3654–3670. https://doi.org/10.1002/joc.3933

Bewket W, Conway D (2007) A note on the temporal and spatial variability of rainfall in the drought-prone Amhara region of Ethiopia. Int J Climatol (Wiley-Blackwell) 27(11):1467–1477. https://doi.org/10.1002/joc.1481

Chen J, Brissette FP, Leconte R (2011) Uncertainty of downscaling method in quantifying the impact of climate change on hydrology. J Hydrol (Elsevier B.V.) 401(3–4):190–202

Christensen JH, Carter TR, Rummukainen M, Amanatidis G (2007) Evaluating the performance and utility of regional climate models: the PRUDENCE project. Clim Change 81(Suppl 1):1–6. https://doi.org/10.1007/s10584-006-9211-6

Conway D, Mould C, Bewket W (2004) Over one century of rainfall and temperature observations in Addis Ababa, Ethiopia. Int J Climatol 24(1):77–91. https://doi.org/10.1002/joc.989

Cubasch U, Meehl GA, Boer GJ, Stouffer RJ, Dix M, Noda a., Senior C a., Raper S, Yap KS. 2001. Projections of future climate change. In: Houghton JT, Ding Y, Griggs DJ, Noguer M, Van der Linden PJ, Dai X, Maskell K, Johnson CA (eds) Climate change 2001. The Scientific Basis: Contribution of Working Group I to the third assessment report of the intergovernmental panel, pp 526–582

Daksiya V, Mandapaka P, Lo EYM (2017) A comparative frequency analysis of maximum daily rainfall for a SE Asian region under current and future climate conditions. Adv Meteorol 2017:16. https://doi.org/10.1155/2017/2620798

Dibike YB, Coulibaly P (2005) Hydrologic impact of climate change in the Saguenay watershed: comparison of downscaling methods and hydrologic models. J Hydrol (Elsevier) 307(1–4):145–163. https://doi.org/10.1016/J.JHYDROL.2004.10.012

Dibike YB, Gachon P, St-Hilaire A, Ouarda TB, Nguyen VT (2008) Uncertainty analysis of statistically downscaled temperature and precipitation regimes in Northern Canada. Theor Appl Climatol 91(1–4):149–170. https://doi.org/10.1007/s00704-007-0299-z

Dile YT, Berndtsson R, Setegn SG (2013) Hydrological response to climate change for Gilgel Abay River, in the Lake Tana Basin—Upper Blue Nile Basin of Ethiopia. PLoS ONE 8(10):12–17. https://doi.org/10.1371/journal.pone.0079296

Ebrahim GY, Jonoski A, van Griensven A, Di Baldassarre G (2013) Downscaling technique uncertainty in assessing hydrological impact of climate change in the Upper Beles River Basin, Ethiopia. Hydrol Res 44(2):377. https://doi.org/10.2166/nh.2012.037

Endris HS, Omondi P, Jain S, Lennard C, Hewitson B, Chang'a L, Awange JL, Dosio A, Ketiem P, Nikulin G, Panitz HJ, Büchner M, Stordal F, Tazalika L (2013) Assessment of the performance of CORDEX regional climate models in simulating East African rainfall. J Clim 26(21):8453–8475. https://doi.org/10.1175/JCLI-D-12-00708.1

Feyissa G, Zeleke G, Bewket W, Gebremariam E (2018) Downscaling of future temperature and precipitation extremes in Addis Ababa under climate change. Climate 6(3):58. https://doi.org/10.3390/cli6030058

Gagnon S, Singh B, Rousselle J, Roy L (2006) An application of the statistical downscaling model (SDSM) to simulate climatic data for streamflow modelling in Québec. Can Water Resour J 30:297–313

Giorgi F, Jones C, Asrar GR (2009) Addressing climate information needs at the regional level: the CORDEX framework. World Meteorol Org Bull 58(3):175–183

Goly A, Teegavarapu RSV, Mondal A (2014) Development and evaluation of statistical downscaling models for monthly precipitation. Earth Interact 18(18):1–28. https://doi.org/10.1175/EI-D-14-0024.1

Gulacha MM, Mulungu DMM (2017) Generation of climate change scenarios for precipitation and temperature at local scales using SDSM in Wami-Ruvu River Basin Tanzania. Phys Chem Earth (Elsevier Ltd) 100:62–72. https://doi.org/10.1016/j.pce.2016.10.003

Harpham C, Wilby RL (2005) Multi-site downscaling of heavy daily precipitation occurrence and amounts. J Hydrol 312(1–4):235–255. https://doi.org/10.1016/j.jhydrol.2005.02.020

Hasan DSNABPA, Ratnayake U, Shams S, Nayan ZBH, Rahman EKA (2017) Prediction of climate change in Brunei Darussalam using statistical downscaling model. Theor Appl Climatol 2:1–18. https://doi.org/10.1007/s00704-017-2172-z

Hashmi MZ, Shamseldin AY, Melville BW (2011) Comparison of SDSM and LARS-WG for simulation and downscaling of

extreme precipitation events in a watershed. Stoch Environ Res Risk Assess 25(4):475–484. https://doi.org/10.1007/s00477-010-0416-x

Hassan Z, Harun S (2011) Statistical downscaling for climate change scenarios of rainfall and temperature. United Kingdom-Malaysia-Ireland Engineering Science Conference 2011 (UMIES 2011)

Hassan Z, Shamsudin S, Harun S (2014) Application of SDSM and LARS-WG for simulating and downscaling of rainfall and temperature. Theor Appl Climatol 116(1–2):243–257. https://doi.org/10.1007/s00704-013-0951-8

Hely C, Bremond L, Alleaume S, Smith B, Sykes TM, Guiot J (2006) Sensitivity of African biomes to changes in the precipitation regime. Glob Ecol Biogeogr 15:258–270

Hessami M, Gachon P, Ouarda TBMJ, St-Hilaire A (2008) Automated regression-based statistical downscaling tool. Environ Model Softw 23(6):813–834. https://doi.org/10.1016/j.envsoft.2007.10.004

Hewitson BC, Crane RG (1996) Climate downscaling: techniques and application. Clim Res 7:85–95

Huang J, Zhang J, Zhang Z, Xu C, Wang B, Yao J (2011) Estimation of future precipitation change in the Yangtze River basin by using statistical downscaling method. Stoch Environ Res Risk Assess 25(6):781–792. https://doi.org/10.1007/s00477-010-0441-9

Hulme M, Doherty R, Ngara T, New M, Lister D (2001) African climate change: 1900–2100. Clim Res 17(2 Special 8):145–168. https://doi.org/10.3354/cr017145

IPCC (2013) Summary for policymakers. Climate change 2013: the physical science basis. Contribution of Working Group I to the Fifth Assessment Report of the Intergovernmental Panel on Climate Change 33. https://doi.org/10.1017/cbo9781107415324

IPCC (2014) Climate change 2014: mitigation of climate change, pp 4–5. Www.Ipcc.Sh

Jain SK, Goswami A, Saraf AK (2009) Assessment of snowmelt runoff using remote sensing and effect of climate change on runoff. Water Resour Manag 24:1763–1777

Jha B, Hu ZZ, Kumar A (2014) SST and ENSO variability and change simulated in historical experiments of CMIP5 models. Clim Dyn 42(7–8):2113–2124

Kharel G, Kirilenko A (2018) Comparing CMIP-3 and CMIP-5 climate projections on flooding estimation of Devils Lake of North Dakota, USA. PeerJ. https://doi.org/10.7717/peerj.4711

King LMM, Irwin S, Sarwar R, McLeod AIA, Simonovic SPP (2012) The effects of climate change on extreme precipitation events in the upper thames river basin: a comparison of downscaling approaches. Can Water Resour J 37(3):253–274. https://doi.org/10.4296/cwrj2011-938

Knutti R, Sedláček J (2013) Robustness and uncertainties in the new CMIP5 climate model projections. Nat Clim Change (Nature Publishing Group) 3(4):369–373. https://doi.org/10.1038/nclimate1716

Kumar D, Kodra E, Ganguly AR (2014) Regional and seasonal intercomparison of CMIP3 and CMIP5 climate model ensembles for temperature and precipitation. Clim Dyn 43(9–10):2491–2518. https://doi.org/10.1007/s00382-014-2070-3

Liu L, Liu Z, Ren X, Fischer T, Xu Y (2011) Hydrological impacts of climate change in the Yellow River Basin for the 21st century using hydrological model and statistical downscaling model. Quat Int (Elsevier Ltd and INQUA) 244(2):211–220. https://doi.org/10.1016/j.quaint.2010.12.001

Maraun D, Wetterhall F, Chandler RE, Kendon EJ, Widmann M, Brienen S, Rust HW, Sauter T, Themeßl M, Venema VKC, Chun KP, Goodess CM, Jones RG, Onof C, Vrac M, Thiele-Eich I (2010) Precipitation downscaling under climate change: recent developments to bridge the gap between dynamical models and the end user. Rev Geophys 48:1–38. https://doi.org/10.1029/2009rg000314.1.introduction

Mearns LO (2009) Methods of downscaling future climate information and applications. White Paper. National Center for Atmospheric Research. Retrieved from www.narccap.ucar.edu/users/user-meeting-09/talks/Downscaling_summary_for_NARCCAP_Users_Meet09.pdf

Mekonnen DF, Disse M (2018) Analyzing the future climate change of Upper Blue Nile River Basin (UBNRB) using statistical down scaling techniques. Hydrol Earth Syst Sci Discuss. https://doi.org/10.5194/hess-2016-543

Semenov MA, Barrow EM (1997) Use of a stochastic weather generator in the development of climate change scenarios. Clim Change 35(4):397–414. https://doi.org/10.1023/A:1005342632279

Semenov MA, Barrow EM (2002) A stochastic weather generator for use in climate impact studies. User Manual, Hertfordshire, UK (August)

Setegn SG, Srinivasan R, Dargahi B (2008) Hydrological modelling in the Lake Tana Basin, Ethiopia Using SWAT Model. Open Hydrol J 2(1):49–62. https://doi.org/10.2174/1874378100802010049

Setegn SG, Rayner D, Melesse AM, Dargahi B, Srinivasan R (2011) Impact of climate change on the hydroclimatology of Lake Tana Basin, Ethiopia. Water Resour Res 47(4):1–13. https://doi.org/10.1029/2010WR009248

Shongwe ME, van Oldenborgh GJ, van den Hurk BJJM, de Boer B, Coelho CAS, van Aalst MK (2009) Projected changes in mean and extreme precipitation in Africa under global warming. Part I: Southern Africa. J Clim 22(13):3819–3837. https://doi.org/10.1175/2009jcli2317.1

Singh V, Goyal MK (2016) Analysis and trends of precipitation lapse rate and extreme indices over north Sikkim eastern Himalayas under CMIP5ESM-2M RCPs experiments. Atmos Res (Elsevier B.V.) 167:34–60. https://doi.org/10.1016/j.atmosres.2015.07.005

Smid M, Costa AC, Costa AC (2018) Climate projections and downscaling techniques : a discussion for impact studies in urban systems. Int J Urban Sci (Taylor & Francis) 22(3):277–307. https://doi.org/10.1080/12265934.2017.1409132

Su F, Duan X, Chen D, Hao Z, Cuo L (2013) Evaluation of the global climate models in the CMIP5 over the Tibetan Plateau. J Clim 26(10):3187–3208

Tofiq FA, Guven A (2014) Prediction of design flood discharge by statistical downscaling and general circulation models. J Hydrol 517:1145–1153

Vallam P, Qin XS (2017) Projecting future precipitation and temperature at sites with diverse climate through multiple statistical downscaling schemes. Theor Appl Climatol. https://doi.org/10.1007/s00704-017-2299-y

Wilby RL, Dawson CW (2004) Using SDSM version 3.1—a decision support tool for the assessment of regional climate change impacts. Environment 17:147–159

Wilby RL, Dawson CW (2013) The statistical downscaling model: insights from one decade of application. Int J Climatol 33(7):1707–1719. https://doi.org/10.1002/joc.3544

Wilby RL, Charles SP, Zorita E, Timbal B, Whetton P, Mearns LO (2004) Guidelines for use of climate scenarios developed from statistical downscaling methods. Analysis 27(August):1–27

Wu R, Chen J, Wen Z (2013) Precipitation-surface temperature relationship in the IPCC CMIP5 models. Adv Atmos Sci 30(3):766–778. https://doi.org/10.1007/s00376-012-2130-8

Yimer G, Jonoski A, Griensven AV (2009) Hydrological response of a catchment to climate change in the Upper Beles River Basin, Upper Blue Nile, Ethiopia. Nile Basin Water Eng Sci Mag Spec Issue Clim Water 2:49–59

Publisher's Note Springer Nature remains neutral with regard to jurisdictional claims in published maps and institutional affiliations.